IntelliTorque

ATR

MetaStation 4E

Family of Rheometers

Brabender®

follow us

MORE INFO

SCAN ME

50 East Wesley Street | South Hackensack, NJ. 07606
chemicalsales@cwbrabender.com | 201-343-8425

Received: 6 December 2019 | Revised: 21 January 2020 | Accepted: 6 February 2020

DOI: 10.1002/pc.25548

RESEARCH ARTICLE

Polymer COMPOSITES WILEY

The role of winding pattern on filament wound composite cylinders under radial compression

Tales V. Lisbôa[1] | **José Humberto S. Almeida Jr**[1,2] | **Ingo H. Dalibor**[3] | **Axel Spickenheuer**[1] | **Rogério J. Marczak**[4] | **Sandro C. Amico**[3,4]

[1]Mechanics and Composite Materials Department, Leibniz Institute of Polymer Research, Dresden, Germany

[2]Mechanical Engineering Department, Aalto University, Espoo, Finland

[3]PPGE3M, Federal University of Rio Grande do Sul, Porto Alegre, Brazil

[4]PROMEC, Federal University of Rio Grande do Sul, Porto Alegre, Brazil

Correspondence
Tales V. Lisbôa, Mechanics and Composite Materials Department, Leibniz Institute of Polymer Research, Dresden, Germany.
Email: tales-lisboa@ipfdd.de

Funding information
Alexander von Humboldt-Stiftung; Conselho Nacional de Desenvolvimento Científico e Tecnológico, Grant/Award Numbers: 0649/2017-0, 424426/2016-1; Coordenação de Aperfeiçoamento de Pessoal de Nível Superior, Grant/Award Number: 1303477; Deutscher Akademischer Austauschdienst, Grant/Award Number: 57447163; Fundação de Amparo à Pesquisa do Estado do Rio Grande do Sul, Grant/Award Number: 17/2551-0001

Abstract

Filament wound (FW) structures present a geometric characteristic in their helical layers: the winding pattern. The pattern, however, is usually disregarded in conventional experimental or numerical approaches even though it can affect the behavior of FW structures, and most studies that account for the pattern are only theoretical. This study aims at deepening the understanding of pattern effects via a comprehensive experimental campaign focusing on composites cylinders under radial compression. Ten winding patterns were considered, from 1 to 10 units along the circumferential direction. Strength, stiffness, absorbed energy and failure mechanisms were evaluated. The results show that the pattern may have a strong influence on both maximum bearing load and absorbed energy, whereas stiffness is less affected.

KEYWORDS

filament winding, radial compression, stiffness, winding pattern

1 | INTRODUCTION

Filament winding (FW) is one of the most suitable manufacturing processes for closed cylindrical structures since continuous fiber tows are deposited onto a rotating mandrel,[1,2] being commonly used for the production of pipes, tubes, shafts, pressure vessels, among others.[3,4,5] The process allows high precision in fiber positioning, high fiber volume fraction and low void content.[6,7] Moreover, based on the winding angle and the superposition of layers, the designer controls thickness, strength and stiffness of the structure.[3]

Several studies have been carried out on the mechanical behavior of FW components. Zu et al.[1] focused on continuum theory and nongeodesic trajectories to optimize shapes of pressure vessel domes, and later Zu et al.[8] addressed the optimum design of pressure vessels for

nongeodesic trajectories and achieved good agreement with experimental results. Bai et al.[9] implemented a progressive damage model based on 3D Hashin failure mode to analyze composite pressure vessels and found good agreement between numerical and experimental results. Almeida Jr. et al.[7] developed a damage model to predict the mechanical response of FW tubes under external pressure and radial compression[10] and found very good correlation between numerical and experimental results. Raffie et al.[11] performed a similar study but applied for tubes under internal pressure, using Hashin's failure criterion for both ply-discount method and continuum damage mechanics approaches. And Eggers et al.[12] analyzed the influence of some FW parameters on the behavior of rings subjected to radial and axial compression, and hoop tensile loading, and reported dominant failure modes as delamination, delamination with minor off-axis cracks, fiber/matrix debonding with fiber breakage, respectively.

An inherent geometric parameter in FW is the pattern formation due to the repetitive and regular winding movements. The pattern is defined as an integer number of diamond-shaped regions on the periphery of the mandrel/liner in the circumferential direction. These shapes are depicted in Figure 1. Inside any diamond, two triangles divided by the inter-crossing region have either $[-\alpha/+\alpha]$ or $[+\alpha/-\alpha]$, where α is the winding angle. Locally, these laminate configurations - anti-symmetric - may change the stress distribution, which may also modify the mechanical behavior of the component. The number of tows required for a particular degree of coverage as well as the possible patterns that can be constructed are defined by solving a diophantine-like equation.[3,4,13] And, by setting the winding angle and the cylinder radius, for instance, one may achieve different degrees of coverage since a variable number of tows are required to produce a particular pattern.

In spite of obtaining good agreement between experimental and numerical results, none of the aforementioned reports have taken into account the pattern in their approaches. Indeed, just a few reports in the literature focus on the influence of the winding pattern on the mechanical behavior of filament-wound components. Among them, Rousseau et al.[14] investigated the influence of the degree of interweaving on the damage behavior of glass/epoxy tubes for different loading cases. For tensile tests and pure internal pressure, the pattern did not show a significant effect, whereas for closed-end internal pressure and weeping, the interweaving induced high concentration of cracks close to the crossover regions. Morozov[5] numerically investigated the influence of winding pattern on thin-walled tubes under internal pressure and concluded that the stress fields in shells may be underestimated by a stress analysis based on conventional mechanics of laminated structures. Similarly, Mian and Rahman[15] numerically studied domes and concluded that the mosaic patterns have a pronounced effect on the behavior of thin-walled composite shells. Uddin et al.[16] analyzed the stress field in a flywheel for several pattern constructions and also concluded that the stress level could be underestimated if the approach is based on conventional mechanics of laminates. Thus, the pattern may, indeed, influence the mechanical response of thin-walled wound components,[16] although it is less important for thicker shells since the stretching-twisting and bending-shear coupling effects are reduced.

As shown above, most investigations taking into account the winding pattern are numerical studies, apart from the work of Morozov,[5] who performed internal pressure tests. In this context, this study presents a comprehensive investigation of the behavior of filament wound composite cylinders manufactured with various patterns, from 1 to 10 units (diamonds in the circumferential direction), under radial compression aiming at bringing greater experimental evidence on the winding pattern effect.

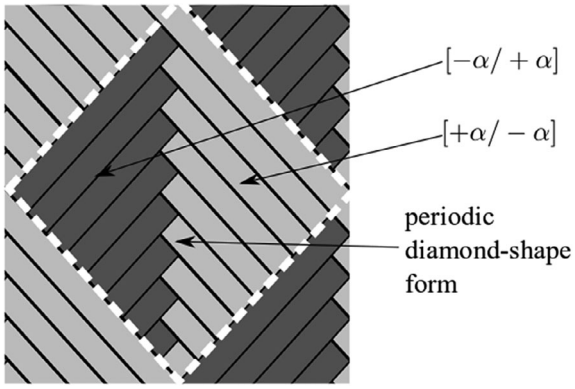

FIGURE 1 Detail of the periodic diamond-shape form and stacking configuration of each side

2 | MANUFACTURING AND TESTING

Towpregs from TCR Composites comprised of Toray T700-12K-50C carbon fiber and UF3369 epoxy resin were used. Design of the cylinders was carried out with CADWIND FW software, with variable winding pattern, p_{tr}, and a constant winding angle of 60°.

A stainless steel-based mandrel with a diameter, ϕ, of 50.8 mm was used, and the geometric characteristics of the produced samples are shown in Table 1. Length and weight were measured and thickness was calculated considering a density of =1430 kg/m^3. Density was determined using Archimedes approach (ASTM D792 standard), where the mass of a specimen is measured in air and also when immersed in distilled water, allowing

the calculation of density. The mean and standard deviations values presented in Table 1 are the mean of 10 measurements for each sample. The degree of coverage parameter, d_c, is an output of the CADWIND software[17] and is calculated as follows:

$$d_c = \frac{b}{p}100\,[\%] \quad (1)$$

where b and p are bandwidth and shift factor, respectively. It was not possible to produce cylinders with the same degree of coverage because this parameter varies based on the defined winding pattern. Nevertheless, the chosen d_c values were as close as possible and not less than 100%, that is, the mandrel is covered with tows with the minimum possible overlap.

In this study, geodesic trajectories were chosen instead of nongeodesic ones because some winding patterns were not feasible via nongeodesic trajectory. For the sake of clarity, although friction between the tow and the mandrel is not considered in geodesic trajectories, a preliminary investigation carried out did not indicate slippage in winding simulations.

The cylinders were produced by dry filament winding using a KUKA 140L100 robot. All cylinders were produced with the same towpreg tension and with the same nominal winding angle throughout the sample. After winding, a shrink tape was wound on the laminate to aid compaction during curing and to minimize void formation. The system (mandrel and laminate) was taken to an oven with air circulation at 105°C for 24 h for curing. Then, the system was cooled down at room temperature, and the mandrel was unscrewed to extract the composite cylinder. A total of ten 1000-mm long cylinders were manufactured, one for each winding pattern studied (the turnaround zones, typical of filament winding, were cut off). The cylinders were cut off in 100-mm long specimens and the edges were polished to ensure parallelism.

The cylinders were subjected to radial compression following recommendations of ASTM D2412 standard for parallel-plate loading of composite cylinders. The tests have been performed in an Instron Universal testing machine model 3382 at a crosshead speed of 5 mm/min, using five cylinders for each winding pattern.

3 | RESULTS AND DISCUSSION

3.1 | Load × displacement curves—characteristics

Figure 2A-J present the load × displacement curves for $p_{tr} = 1$ to $p_{tr} = 10$, respectively. The curves present similar shape for each type of specimen, which indicates that the compressive tests were successfully performed and the samples have good repeatability.

Analysis of Figure 2 reveals that the compressive response varies with the pattern, including the general shape and the maximum supported load. This indicates that the effect of the winding pattern should not be neglected. Regarding the shape of the force × displacement curves, one may classify the responses into three groups. For $p_{tr} = 1, 2, 8, 10$, three main regions are seen, corresponding to quasi-linear, damage propagation and residual failure. For $p_{tr} = 5, 7, 9$, the second region is barely seen, and, for the other patterns ($p_{tr} = 3, 4, 6$), only some specimens display a damage propagation region.

Figure 3A-J show outer and inner surfaces of typical specimens after testing, along with some details of the failure. There are some differences in the outer failure surface for the various patterns, but the inner surface (the region located 90° from the center of the plate's loading) is similar. Based on curved beam theory, maximum bending stress (compressive) occurs at the inner surface leading to catastrophic failure (see Figure 2). The noticeable damage in the outer surface is a result of the loading

TABLE 1 Geometric characteristics of all specimens

p_{tr}	Degree of coverage (%)	Length (mm)	Weight (mm)	Thickness (mm)
1	102.26	99.26 ± 1.08	18.92 ± 0.16	0.822 ± 0.011
2	104.81	98.60 ± 0.95	19.66 ± 0.26	0.859 ± 0.014
3	104.81	98.46 ± 1.31	19.42 ± 0.26	0.850 ± 0.026
4	109.80	98.38 ± 0.70	20.36 ± 0.31	0.891 ± 0.015
5	112.48	98.28 ± 1.37	20.62 ± 0.25	0.903 ± 0.016
6	104.81	98.78 ± 1.49	19.42 ± 0.22	0.847 ± 0.016
7	120.15	98.68 ± 0.81	19.32 ± 0.13	0.844 ± 0.009
8	112.48	99.74 ± 0.88	22.50 ± 0.17	0.970 ± 0.011
9	125.26	99.42 ± 1.37	20.90 ± 0.18	0.905 ± 0.015
10	104.81	98.34 ± 1.02	23.04 ± 0.23	1.007 ± 0.014

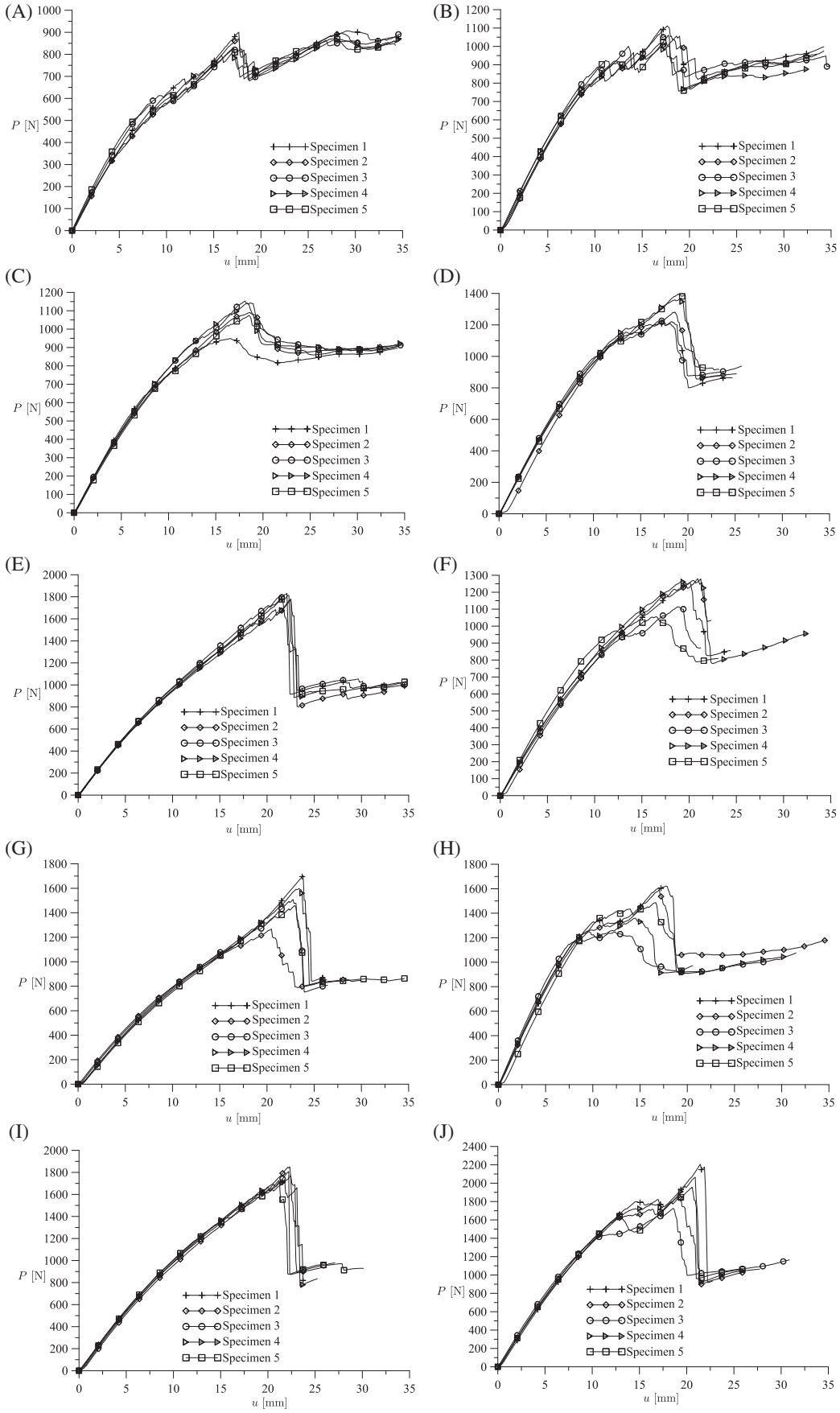

FIGURE 2 Load × displacement curves for specimens with winding pattern of: A: 1/1; B: 2/1; C: 3/1; D: 4/1; E: 5/1; F: 6/1; G: 7/1; H: 8/1; I: 9/1; and J: 10/1. Plots with different axes limits for better visualization

from the applied stress and the friction with the loading plates, which helps explaining the lateral spread in some patterns (eg, Figure 3E,F).

Further interpretation from the curves in Figures 2 and 3 can be drawn, as follows:

- $p_{tr} = 1$ (Figure 2A): Compared to the other patterns, the first failure is noticed earlier, and so is damage propagation. The first identifiable failure occurs at ≈550 N, but the cylinder kept supporting the load. The first cracks appear in the contacts between the specimen and the loading plates and they propagate towards the lateral of the cylinder. In general, these initial cracks appear in the inner surface of the cylinder and they propagate towards the outer surface. When the cracks start appearing at the lateral of the cylinder, major failure are observed, indicated by the maximum bearing load and subsequent large delamination, with a load drop of ≈20%, even though the samples keep supporting some load up to 35 mm displacement. These cylinders failed predominantly with large transverse cracks due to high stress concentrations on the side region of the cylinders.
- $p_{tr} = 2$ (Figure 2B): It can be noticed that the linear-elastic region for this pattern is longer than for $p_{tr} = 1$, and the first failure is observed at ≈800 N. After that, damage progresses with large off-axis cracks. Ultimate failure load occurs at a displacement level of ≈15 mm. Comparing to $p_{tr} = 1$, it appears that the major cracks grow in the regular laminate areas. Thus, the inter-crossing regions prevent the cracks to propagate, acting as physical barriers, preventing faster crack growing. Another evidence of the pattern effect is the magnitude of the load drops prior to the ultimate failure, which are greater than those for $p_{tr} = 1$. The failure mechanisms of this pattern were very similar to $p_{tr} = 1$.
- $p_{tr} = 3$ (Figure 2C): These curves clearly have a more linear-elastic behavior up to failure and very small load drops prior to the maximum load, which suggest that the cylinders did not present significant damage progression. Here again the cylinders failed by transverse compression and delamination, even though the shape of the curves suggests that minor off-axis cracks dominated global failure. From a physical point of view, there are twice as many inter-crossing areas in this pattern, but the distance between them do not bring a barrier effect to crack propagation. This means that global failure was mostly governed by the laminate itself instead of the inter-crossing areas. In this pattern, the off-axis cracks propagated throughout the length of the cylinder (Figure 3C), suggesting that the inter-crossing areas were not very efficient in retarding crack propagation.
- $p_{tr} = 4$ (Figure 2D): The curve shapes are similar to those of $p_{tr} = 3$, but the ultimate failure load is higher and a "shoulder" is seen in all 5 specimens near ≈1110 N. The load then slowly increased up to the final failure. The global behavior can be associated to the greater degree of coverage and thickness. Similarly to $p_{tr} = 3$, failure was triggered at the inner surface followed by a large longitudinal transverse crack which dominated final failure.
- $p_{tr} = 5$ (Figure 2E): This winding pattern showed the most linear-elastic characteristic, and all samples failed in a more brittle manner, with no clear damage progression. Also, the maximum supported load is the highest so far, which implies that this degree of interweaving is efficient in preventing failure initiation. Although the failure mechanisms observed in Figure 3E are not very different from the other patterns, the cracks only appeared near the final failure in this case.
- $p_{tr} = 6$ (Figure 2F): The load × displacement curves for this pattern are similar to those for $p_{tr} = 4$, that is, the curve is slightly nonlinear throughout the loading history, with a brittle failure. Differently from $p_{tr} = 2$, several minor cracks along the cylinder were not observed. After a displacement of about 15 mm, the cylinder starts losing stiffness, which can be attributed to its large lateral displacement. The final failure was governed by a "zig-zag like" failure, where the cracks grew along the angle-ply fiber direction on the side region of the cylinder.
- $p_{tr} = 7$ (Figure 2G): This pattern shows a very particular behavior since the samples gain stiffness up to ≈8 mm, and then progressively lose it until several minor load drops appear. However, it is important to mention that this pattern has a degree of coverage of 120.15%, which favors ultimate load increase. In these specimens, the major cracks did not take place exactly on the side of the cylinder, instead they appeared between the side and the bottom of the cylinder (in contact with the compressive plate), justifying the "slenderness" shape of the load × displacement curve before failure initiation. In this case, the cracks propagated transversely along the length of the cylinder.
- $p_{tr} = 8$ (Figure 2H): There is not much difference among the patterns 8–10. Thus, for such small sized diamond units, the mechanical response of the cylinders is less dependent on their winding patterns. This range of patterns can also lead to undesired manufacturing defects or deviations from the programmed winding path, such as gaps, overlaps and fiber misalignment. The load evolves linearly up to ≈8 mm followed by an increase in cylinder stiffness, which has a positive effect on the overall response, where loads close to 1600 N are reached, with less material than $p_{tr} = 7$, for instance. Their failure

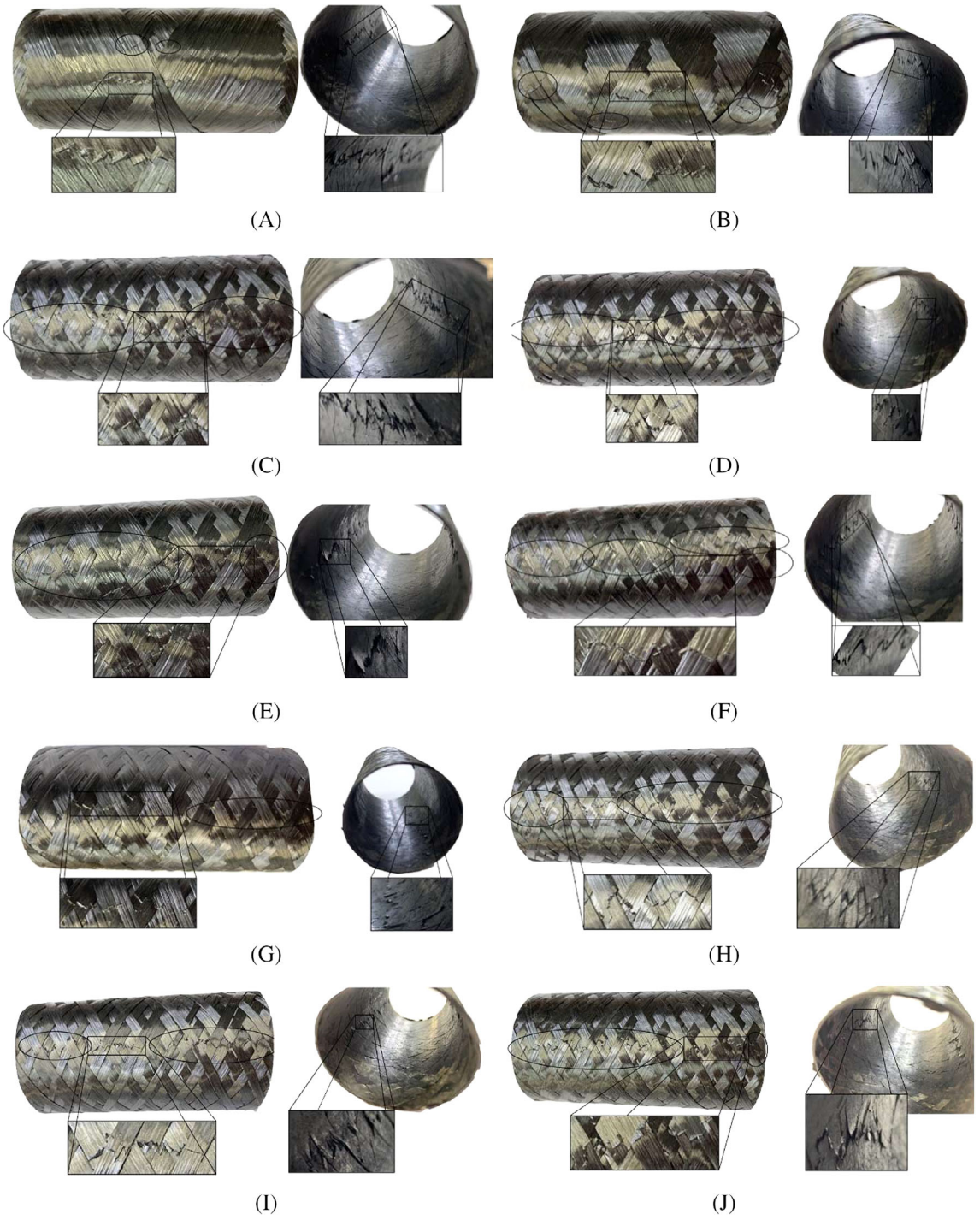

FIGURE 3 Fractured specimens with winding pattern of: A: 1/1; B: 2/1; C: 3/1; D: 4/1; E: 5/1; F: 6/1; G: 7/1; H: 8/1; I: 9/1; and J: 10/1 [Color figure can be viewed at wileyonlinelibrary.com]

mechanism also follows the theory of curved beams, where failure tends to initiate on the side region of the curved beam.

- $p_{tr} = 9$ (Figure 2I): This pattern yielded a very similar behavior to $p_{tr} = 5$ and $p_{tr} = 7$, but supporting higher loads. A slight difference is observed close to ultimate failure, where several minor load drops are identified and attributed to transverse cracks around the cylinder. This pattern favors a linear-elastic behavior followed by sudden failure at high load levels, with a major crack propagating outwards in the whole length of the cylinder.
- $p_{tr} = 10$ (Figure 2J): Similarly to $p_{tr} = 8$, stiffening is observed after a displacement of ≈10 mm, with a

positive effect on maximum load. Perhaps the great number of small units may prevent delamination and crack propagation of transverse cracks along the cylinder and, hence, enhance the load-carrying ability of this winding pattern. And the damage mechanism was almost the same of $p_{tr} = 9$.

It is worth noticing that crack propagation does not follow a "straight" line, which would be expected for isotropic materials. In both internal and external surfaces, crack propagates parallel to the boundaries of the tows or perpendicular to it (inside a particular tow). For that reason, the propagation of the crack has a "zig-zag" shape, which is best observed at the internal surface (details in Figure 3).

3.2 | Stiffness

As shown in Table 1, length and thickness varied with the pattern, and can therefore mislead the findings related to cylinder stiffness. In order to more suitably compare the results, a correction factor based on these parameters is proposed here. Using an analytical approach for the stiffness of rings under parallel plate compression, as presented in ref. [18], a correction factor, $\hat{k}$, is calculated by

$$\hat{k} = \frac{k}{E} = \frac{8\pi IA}{(\pi^2 - 8)Ar^3 + \pi^2 Ir} \tag{2}$$

where,

$$A = Lt\, I = \frac{Lt^3}{12}\, r = r_i + t \tag{3}$$

and L, t and r_i correspond to length, thickness, and inner radius (mandrel radius), respectively; I and A stand for cylinder wall cross-section moment of inertia and area, respectively. E is the Young modulus and it is included in the correction function since the material influence is expected to be the same for all specimens (same material and winding angle). Equation (2) is based on the assumption that thickness is much smaller than radius (minimum value of ≈4% in this study) and the contact angle between plate and cylinder is small. The calculated $\hat{k}$ values for each pattern are shown in Table 2.

Stiffness is defined as the slope of the secant line that crosses the points $(u(1), f(1))$ and $(u(2), f(2))$, for each force × displacement curve. In order to minimize the influence of local data fluctuations, these points are also interpolated by the closest points of $u = 0.95$ and $u = 1.05$ mm for $(u(1), f(1))$ as well as $u = 1.95$ mm and $u = 2.05$ mm for $(u(2), f(2))$. That is, the slope, k, is obtained from

$$k = \frac{f(2) - f(1)}{u(2) - u(1)} = f(2) - f(1) \tag{4}$$

Figure 4 presents both average and weighted values of stiffness. When analyzing Figure 4B, one should focus on the variation in values with respect to the pattern, instead of the values themselves. When weighted, stiffness varies only slightly, within the deviation, that is, the filament wound tubes of all patterns exhibit similar stiffness. This could be expected since material, fiber orientation, mass and geometric parameters are comparable (after the correction). Interestingly, $p_{tr} = 1$ and $p_{tr} = 8$ have the lowest and highest stiffnesses, respectively. These variations may be related to the degree of coverage (which is the lowest for $p_{tr} = 1$), and also partly justifies the largest stiffness of $p_{tr} = 8$.

In order to statistically evaluate this hypothesis, the t test was applied to the weighted stiffness results for the various patterns. The achieved P-values are shown in Table 3, where black and red numbers define P values $>.05$ and $\leq.05$, respectively. It is noticeable that $p_{tr} = 8$ has a corrected stiffness statistically different from all other patterns, whereas $p_{tr} = 1$ is similar to four other patterns. Moreover, the P values for $p_{tr} = \{2\ 3\ 4\ 5\ 6\ 7\ 9\ 10\}$ are large (≥ 0.1) in most cases, that is, the t-tests suggest that the corrected stiffnesses are similar for these patterns.

3.3 | Maximum load and energy to failure

Another important parameter that can be analyzed from the curves in Figure 2 is the maximum load supported by the specimens, which have been compiled in Figure 5. No correlation factor has been analyzed for this parameter since distinct failure mechanisms take place together, as discussed before.

TABLE 2 Values of $\hat{k}$ for each pattern ($\delta\hat{k}$ is the propagated SD)

p_{tr}	1	2	3	4	5	6	7	8	9	10
$\hat{k}$	3.589	4.063	3.931	4.516	4.694	3.907	3.856	5.875	4.775	6.461
$\delta\hat{k}$	0.150	0.197	0.221	0.224	0.259	0.221	0.123	0.206	0.236	0.277

It is clearly noticeable that maximum load differs between patterns. However, no clear trend could be identified. For example, patterns with 5, 9, and 10 units resisted approximately 100% more load then $p_{tr} = 1$, with a slightly large mass, whereas $p_{tr} = 4$ has almost the same dimensions and mass of $p_{tr} = 5$ but resisted ≈28% less. Nevertheless, one may notice that the patterns with smaller regions of damage propagation previous to the major load drop (failure) yield higher final loads.

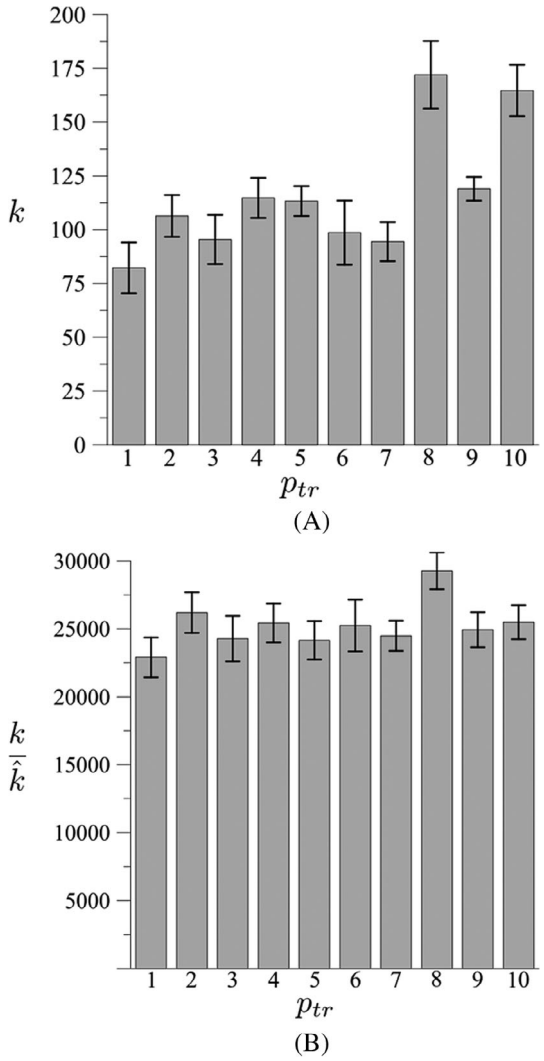

FIGURE 4 Average stiffness, A, and average weighted stiffness, B, for all specimens

The absorbed energy to failure, based on the area of the force × displacement curves from the origin to the displacement at the first major load drop, was also analyzed. The trapezoidal rule is used to find the area under the curves and the energy is divided by the volume of the cylinders in order to compare the different patterns in an equal basis (specific energy—Figure 6). The patterns can be divided into three groups concerning the amount of absorbed energy to failure: $p_{tr} = \{5, 7, 9, 10\} > p_{tr} = \{4, 6, 8\} > p_{tr} = \{1, 2, 3\}$.

4 | CONCLUSION

This study investigated the influence of the winding pattern on the response of cylinders under radial compression. The studied patterns varied from 1-unit to 10-units, but the winding angle was kept constant (60°).

From the load × displacement curves, a clear difference on the mechanical response of the specimens with different patterns was observed, where patterns $p_{tr} = 1$, $p_{tr} = 2$, and $p_{tr} = 6$ yielded progressive damage followed by delamination, and patterns $p_{tr} = 5$, $p_{tr} = 7$, and $p_{tr} = 9$ failed in a brittle manner, with failure governed by transverse cracks on the side of the cylinders. The other patterns presented more complex failure mechanisms, what might be related to manufacturing characteristics, such as voids and resin pockets. A correction factor was proposed to normalize stiffness of the cylinders to take into account their distinct dimensions. Results of *t* tests indicated that corrected stiffness is similar for all patterns, except for $p_{tr} = 1$ and $p_{tr} = 8$. Maximum load and energy

TABLE 3 *T* -test for the corrected stiffness

	1	2	3	4	5	6	7	8	9	10
1	1.000	0.008	0.206	0.025	0.209	0.061	0.090	0.000	0.048	0.017
2		1.000	0.093	0.434	0.058	0.407	0.075	0.009	0.191	0.444
3			1.000	0.276	0.901	0.419	0.821	0.001	0.507	0.230
4				1.000	0.194	0.867	0.279	0.002	0.580	0.945
5					1.000	0.334	0.688	0.000	0.388	0.152
6						1.000	0.465	0.005	0.769	0.816
7							1.000	0.000	0.574	0.217
8								1.000	0.001	0.002
9									1.000	0.507
10										1.000

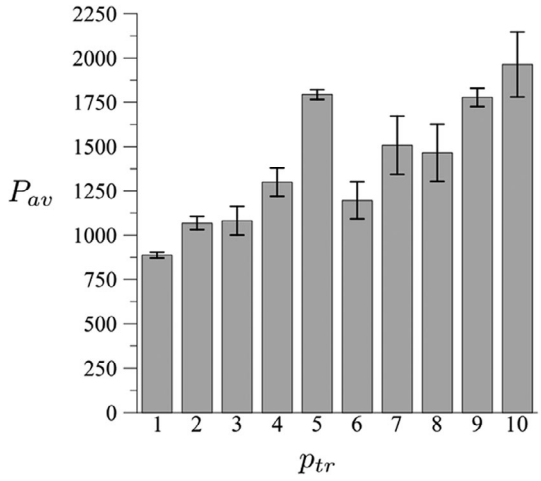

FIGURE 5 Maximum supported load for all winding patterns

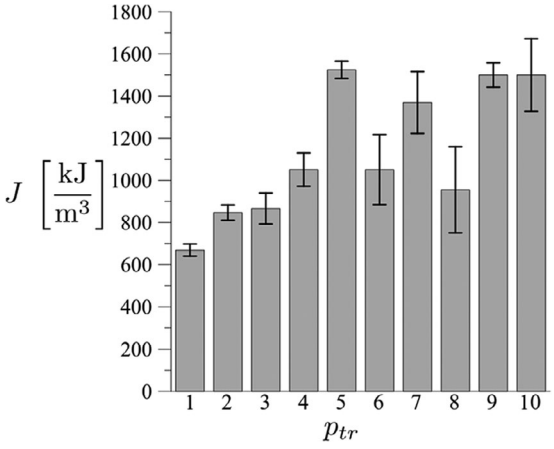

FIGURE 6 Absorbed energy for all studied cylinders

to failure presented more prominent differences among the patterns, and those patterns that displayed catastrophic failure (p_{tr}= 5, 7, 9, 10) without noticeable damage progression tended to absorb more energy at break.

In all, stiffness did not significantly change among the patterns, whereas the shape of load × displacement curves, the maximum supported load and energy at break were dependent on the pattern. Thus, the pattern can indeed affect the compressive response of filament wound structures and its influence should not be disregarded.

ACKNOWLEDGEMENTS

The authors are grateful to CNPq (Universal project numbers 424426/2016-1 and 0649/2017-0); FAPERGS (PqG project number 17/2551-0001); CAPES (PROBRAL project number 88881.198774/2018-01); and Alexander von Humboldt Foundations for the financial support.

ORCID

Tales V. Lisbôa https://orcid.org/0000-0003-1026-6243
José Humberto S. Almeida Jr https://orcid.org/0000-0002-9408-7674
Sandro C. Amico https://orcid.org/0000-0003-4873-2238

REFERENCES

[1] L. Zu, S. Koussios, A. Beukers, *Compos. A: Appl. Sci. Manuf.* **2010**, *41*(9), 1312. https://doi.org/10.1016/j.compositesa.2010.05.015.
[2] V. Vasiliev, E. Morozov, *Mechanics and Analysis of Composite Materials*, Oxford, UK: Elsevier Science Ltd., **2001**.
[3] I. H. Dalibor, T. V. Lisboa, R. J. Marczak, S. C. Amico, *J. Br. Soc. Mech. Sci. Eng.* **2019**, *41*, 576. https://doi.org/10.1007/s40430-019-2083-2.
[4] S. T. Peters, *Composite Filament Winding*, ASM International, Materials Park **2011**.
[5] E. Morozov, *Compos. Structures* **2006**, *76*(1–2), 123. https://doi.org/10.1016/j.compstruct.2006.06.018.
[6] J. H. S. Almeida Jr., H. Faria, A. T. Marques, S. C. Amico, *J. Reinforced Plastics Compos.* **2014**, *33*(24), 2274. https://doi.org/10.1177/0731684414560221.
[7] J. H. S. Almeida Jr., M. L. Ribeiro, V. Tita, S. C. Amico, *Mater. Des.* **2016**, *96*, 431. https://doi.org/10.1016/j.matdes.2016.02.054.
[8] L. Zu, H. Xu, H. Wang, B. Zhang, B. Zi, *Compos. Struct.* **2019**, *207*, 41. https://doi.org/10.1016/j.compstruct.2018.09.007.
[9] H. Bai, B. Yang, H. Hui, Y. Yang, Q. Yu, Z. Zhou, P. Xian, *Polym. Compos.* **2019**, *40*, 4427. https://doi.org/10.1002/pc.25304.
[10] J. H. S. Almeida Jr., M. L. Ribeiro, V. Tita, S. C. Amico, *Compos. Struct.* **2017**, *160*, 204. https://doi.org/10.1016/j.compstruct.2016.10.036.
[11] R. Rafiee, M. A. Torabi, S. Maleki, *Polym. Test.* **2018**, *67*, 322. https://doi.org/10.1016/j.polymertesting.2018.03.020.
[12] F. Eggers, J. H. S. Almeida Jr., C. B. Azevedo, S. C. Amico, *Polym. Test.* **2019**, *78*, 105951. https://doi.org/10.1016/j.polymertesting.2019.105951.
[13] B. S. Johansen, A. Lystrup, M. Jensen, *J. Mater. Process. Technol.* **1998**, *77*(1–3), 194. https://doi.org/10.1016/S0924-0136(97)00417-2.
[14] J. Rousseau, D. Perreux, N. Verdi`ere, *Compos. Sci. Technol.* **1999**, *59*(9), 1439. https://doi.org/10.1016/S0266-3538(98)00184-5.
[15] H. H. Mian, H. Rahman, *Int. J. Struct. Integ.* **2011**, *2*(3), 345. https://doi.org/10.1108/17579861111162932.
[16] M. S. Uddin, E. V. Morosov, K. Shankar, *Compos. Struct.* **2014**, *107*, 260. https://doi.org/10.1016/j.compstruct.2013.07.004.
[17] CADWIND User Manual – MATERIAL SA (**2007**).
[18] A. Gasmi, P. F. Joseph, T. B. Rhyne, S. M. Cron, *Int. J. Solids Struct.* **2011**, *48*(5), 843. https://doi.org/10.1016/j.ijsolstr.2010.11.018.

How to cite this article: Lisbôa TV, Almeida Jr JHS, Dalibor IH, Spickenheuer A, Marczak RJ, Amico SC. The role of winding pattern on filament wound composite cylinders under radial compression. *Polym Compos*. 2020;41:2446–2454. https://doi.org/10.1002/pc.25548